Extended Hückel theory for bandstructure, chemistry, and transport. II. Silicon

D. Kienle, J.I. Cerda, K.H. Bevan, G-C. Liang, L. Siddiqui, and A.W. Ghosh

¹Purdue University, Department of Electrical and Computer Engineering, West Lafayette, IN 47907, USA
²Instituto de Ciencia de Materiales de Madrid, CSIC, Cantoblanco 28049, Madrid, Spain
³University of Virginia, Department of Electrical and Computer Engineering, Charlottesville, VA 22903, USA
(Dated: September 6, 2013)

In this second paper, we develop transferable semi-empirical parameters for the technologically important material, silicon, using Extended Hückel Theory (EHT) to calculate its electronic structure. The EHT-parameters are optimized to experimental target values of the band dispersion of bulk-silicon. We obtain a very good quantitative match to the bandstructure characteristics such as bandedges and effective masses, which are competitive with the values obtained within an $sp^3d^5s^*$ orthogonal-tight binding model for silicon⁹. The transferability of the parameters is investigated applying them to different physical and chemical environments by calculating the bandstructure of two reconstructed surfaces with different orientations: Si(100) (2x1) and Si(111) (2x1). The reproduced π - and π^* -surface bands agree in part quantitatively with DFT-GW calculations and PES/IPES experiments demonstrating their robustness to environmental changes. We further apply the silicon-parameters to describe the 1D band dispersion of a unrelaxed rectangular silicon nanowire (SiNW) and demonstrate the EHT-approach of surface passivation using hydrogen. Our EHT-parameters thus provide a quantitative model of bulk-silicon and silicon-based materials such as contacts and surfaces, which are essential ingredients towards a quantitative quantum transport simulation through silicon-based heterostructures.

I. INTRODUCTION

Silicon is the dominant component in fabrication of semi-conducting devices and continues to play a key role in future nanoelectronic devices. Recent STM-experiments of molecules to highly doped silicon (n- or p-type doping) showed NDR-behaviour at room temperature in the molecular current-voltage characteristics, which might be a modest initial step towards a molecule based electronics. The NDR-behavior, however, was predicted and theoretically demonstrated by Datta and coworkers using a physical resonable model for the electronic structure of silicon. Therefore, an correct model for the electronic structure of all constituents is essential for a quantitative modeling of quantum transport on nano- and atomistic scales.

DFT-based approaches are well-suited to determine electronic and atomic material properties which depend on the total energy.² Abinitio methods in various approximations such as DFT-LDA/GGA have been successful to describe properties of molecules and metals, 3,4 but they are less benchmarked for the electronic properties of semi-conducting materials, particularly for multiple bandedges and effective masses - both of them are important components for a quantitative simulation of quantum transport. For semi-conductors one well known failure of DFT-LDA/GGA calculations is that the bandgap is systematically underestimated by about a factor of 2,5 which makes a quantitative modeling for example of silicon difficult. Quantitative correct bandgaps can be obtained within the GW-approximation, 6 which is computationally expensive and might thus have limited usage at least for transport through large nanostructures.

At the other end are less rigorous, but computationally

less expensive semi-empirical methods such as orthogonal and non-orthogonal tight binding approaches. Here, the electronic structure is not rigorously calculated, but determined by an optimization of the free parameters such as the matrix elements of the Hamiltonian and overlap to match bandedges and effective masses. Orthogonal tight-binding (OTB) approaches have been extensively developed in the past and further optimized to describe the electronic structure of bulk semi-conductors such as silicon and germanium, for example^{7,8,9}. However, the transferability of the bulk optimized parameters - a problem of any semi-emipirical approach - has not been clearly demonstrated, for example, by calculating the electronic structure of (re-constructed) surfaces of different orientations. In turn, their robustness has been mainly shown for atomic structure optimization of bulk, surfaces, and finite size clusters, which requires the calculation of the total energy. 10,11,12,13,14,15,16 The latter, however, is just an integral property of the band dispersion and eventual errors in the bandstructure cancel.¹⁷

In this paper we use a non-orthogonal tight-binding scheme - Extended Hückel Theory (EHT) - to calculate the electronic structure of the technologically important material silicon. In our first paper, we applied the EHT approach to carbon nanotubes demonstrating the transferability of the EHT-parameters for carbon to small diameter tubes as well as to a strongly deformed CNT-molecule heterostructure. ¹⁸ Here, we present optimized EHT-parameters for bulk-silicon and benchmark its bandstructure against multiple target values such as bandedges and effective masses. We explore the transferability of these EHT-parameters to different environments by calculating the 2D-bandstructure for two reconstruced silicon surfaces, silicon (100) (2x1) and (111)

(2x1), and compare them quantitatively to experiments and state of the art DFT-GW calculations. Finally, we use the silicon parameters to calculate the 1D band dispersion, density-of-states (DOS), and transmission (T) for a un-reconstructed silicon nanowire with and without hydrogen passivation demonstrating the capabilities of Extended Hückel Theory to model passivated surfaces of nanostructures. The EHT-parametrization for silicon is shown to be quite transferable to different environments, so that a quantitative modeling of silicon-based devices becomes feasible.

The paper is organized as follows: section II summarizes briefly the main features of Extended Hückel Theory. The optimized EHT parameters for bulk silicon along with the comparison of the bandedges and effective masses to experimental target values are discussed in section III. We then investigate the transferability of the parameters by employing them to different silicon surfaces. Finally, the 1D electronic structure of a silicon nanowire is determined including its surface passivation, and summarize our work in section IV.

II. APPROACH

The silicon bandstructures for the bulk, the two reconstruced surfaces, and the 1D nanowire are calculated within a non-orthogonal Slater-Koster scheme¹⁹ using Extended Hückel Theory to generate the overlapand Hamiltonian-matrix elements **S** and **H**, respectively. Here, we briefly summarize the essential features of EHT, which is described in more detail in Refs. ^{18,20}.

Extended Hückel Theory is a semi-empirical theory to calculate the electronic structure of molecules and elemental solids. The most striking difference between EHT and orthogonal tight-binding (OTB) is that in EHT one works with explicit atomic-like orbital basis functions (AO), which are used to construct the matrix elements S and H. In turn, in orthogonal-tight binding the basis functions are not known and used as a formal tool to construct all matrix elements of the Hamiltonian. The matrix elements are then usually adjusted to a reference bandstructure, for example. Compared to OTB in Extended Hückel Theory one adjusts only the diagonal matrix elements of the Hamiltonian (onsite energies) and the parameters specifying the basis functions, which are Slater type functions (STO). 18,21 Since the basis functions are known, the overlap matrix S is calculated explicitly and used to construct the off-diagonal matrix elements of the Hamiltonian (hopping) according to ^{18,20}

$$H_{\mu\mu} = E_{\mu\mu} ,$$

$$S_{\mu\nu} = \int d^{3}\mathbf{r} \; \phi_{\mu}^{*}(\mathbf{r}) \; \phi_{\nu}(\mathbf{r}) ,$$

$$H_{\mu\nu} = \frac{1}{2} K_{eht} \; S_{\mu\nu} \left(H_{\mu\mu} + H_{\nu\nu} \right) , \qquad (1)$$

assuming that the Hamiltonian depends linearly on the overlap. 20 The original EHT-prescription, cf. Eq. (1),

can be further generalized, so that heterogeneous systems such as heterostructures and interfaces can be modeled. ^18,22,23 The labels μ,ν refer to the atomic orbitals, and $S_{\mu\nu}$ is the overlap matrix between the orbital basis function ϕ_{μ} and ϕ_{ν} , respectively. K_{eht} is an additional fit parameter usually set to 1.75 for molecules and 2.3 for solids. 20,21 Compared to the formal OTBbasis set, Slater basis functions are non-orthogonal, i.e. $\mathbf{S} \neq \mathbf{I}$, which provides an improved transferability of the model parameters with respect to changes in the environment 4,24,25; the enhanced transferability can be justified by constructing orthogonal Löwdin orbitals from the non-orthogonal basis functions. Compared to the original AO's these Löwdin functions are more longranged to enforce orthogonality among different Löwdin functions over the entire domain. Consequently, the Löwdin basis becomes more sensitive to changes in the actual environment.

A concrete example where the transferability of parameters becomes evident are structural deformations. For bulk-like systems empirical scaling rules have been developed, ²⁶ so that effects of strain on the electronic structure can be studied using an orthogonal tightbinding approach employing the commonly used nearest neighbor approximation (NNA). Even though these empirical approaches for structural deformations are calibrated and work well for bulk systems, the transferability of the bulk-optimized parameters along with the scaling rules have not been tested and benchmarked, for example, for reconstructed silicon surfaces. The difficulty in modeling (reconstructed) surfaces within OTB is that surface reconstruction 1). is usually accompanied by large structural changes beyond 2-5% and 2). is accompanied by bond changes. With respect to point 1). it is not a priori obvious whether the scaling rules remain valid beyond small deformations for which they have been calibrated; regarding point 2). it is questionable if a nearest-neighbor approximation which works for bulk can be consistently applied to reconstructed surfaces. Using empirical scaling rules the hopping matrix elements between neighboring atoms of the deformed structure are usually determined from the bulk hopping matrix element between the same atoms. In the case of the two dimer atoms the problem is that their initial bulk hopping matrix elements is zero, since their distance with ≈ 3.8 Ais larger than the nearest-neighbor cut-off of 2.35 A. However, to reproduce the experimentally observed piand π^* surface bands it is important that the electronic structure model provides the correct hopping matrix elements between the two dimer atoms.

III. RESULTS FOR EHT-ELECTRONIC STRUCTURE FOR SILICON

A. Si-Bulk

To perform quantitative transport calculations through nanostructure materials, the free parameters of a semi-empirical tight-binding model have to be calibrated to experimental targets and/or bandstructure data obtained from other theoretical approaches. For Extended Hückel Theory Cerda and Soria have developed EHT-parameters for several bulk crystal structures such as metals, semi-conductors, and compounds. Specifically, for silicon these parameters have been optimized to match the bulk-dispersion of DFT-GW calculations of Rohlfing $et\ al.^6$ at selected points within the 3D Brillouin zone. ²¹

We start by optimizing the EHT-parameters using experimentally determined bandstructure characteristics of bulk silicon such as bandedges and effective masses as targets. We use the TBGreen code²⁷ to minimize the root-mean square error (RMS) between our EHT-bands and the targets via a conjugate gradient method as described in Ref.²¹. Since most of the targets refer to experiments done at low temperatures (5 – 10 K²⁹), we perform the minimization of the RMS-error at T=0.0 K. The 3D bandstructure of silicon is calculated using a sp^3d^5 orbital basis for each silicon atom. In order to capture and to optimize the split-off gap Δ_0 , the Hamiltonian is spin-dependent through the spin-orbit coupling, LS_p , used as additional fit parameter.

Figure 1 shows the band dispersion for bulk-silicon using the optimized EHT-parameters for a silicon atom.²⁸

In Table I we show the final results of our optimization along with their relative error (2nd and 3rd column) with the experimental target values as reference (3rd column). Our values for the bandedges as well as for the effective masses agree very well with the target values, 29 and are in their quality competitive to the state-of-the art orthogonal $sp^3sd^5s^*$ tight-binding model for bulk-silicon.

B. Si-Surfaces for different Orientations

We now investigate the transferability of our EHT-parameters for bulk-silicon and use them to calculate non-selfconsistently the surface bandstructure for two different surface orientations. The semi-infinite surfaces are modeled by a finite slab consisting of a series of layers. Because of this truncation one introduces an additional free surface at the bottom of the slab and hence unphysical surface states, which can extend towards the true surface and thus tamper the surface band dispersion. To eliminate the dangling bond states at the bottom of the slab we passivate in each case the surface of (100) and (111) orientation by attaching hydrogen.

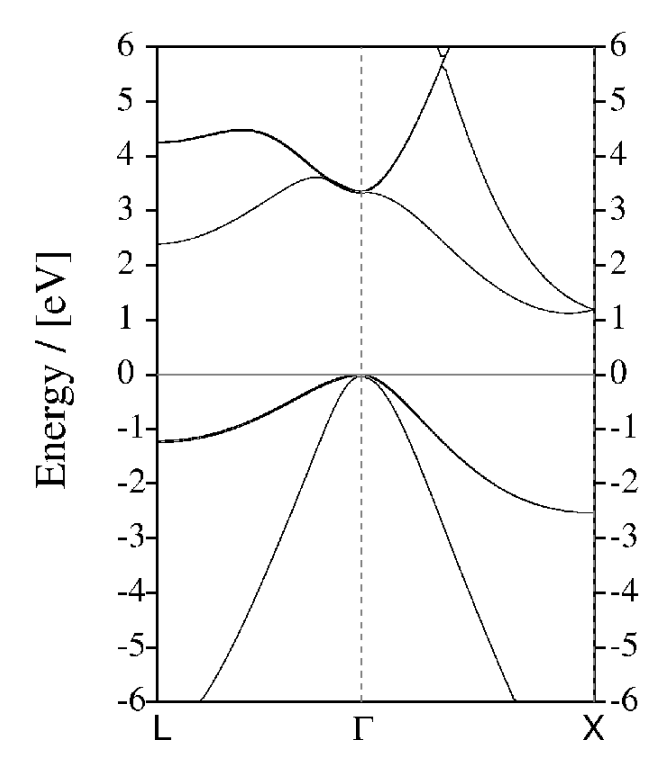


FIG. 1: Bandstructure of bulk-silicon calculated within EHT using the parameters given in Table²⁸ The Fermi level is at $E_F=0.0$ eV as indicated by the horizontal solid line. The EHT parameters are optimized to experimental target values taken from Ref.²⁹.

To calculate the 2D silicon bandstructure of the reconstructed surface we use the unit cell coordinate of Ref.³⁰ for Si(100) (2x1) and for Si(111) (2x1) from Ref.³¹ as shown in Figure 2. For Si (100) (2x1) we use a slab with

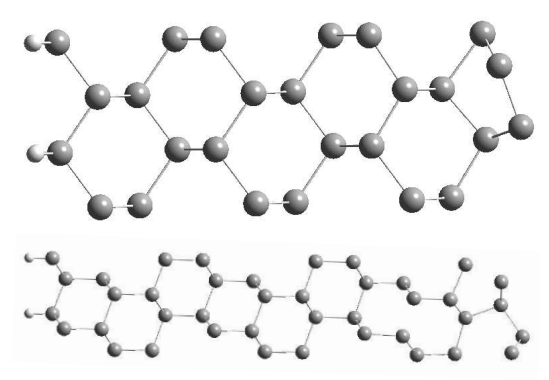


FIG. 2: Structure of the unit cell for the two silicon surfaces. 30,31 . Top:Si(100) (2x1) with the first 4 layers relaxed and 9 bulk-like layers Bottom: Si(111) (2x1) where the first 8 layers are relaxed and 12 bulk layers. In each case, the bottom of the surface is hydrogen passivated to remove dangling bond states.

in total 13 layers, where the first 4 layers correspond to the reconstructed silicon surface, and the remaining 8 layers correspond to positions of bulk silicon. The last layer is hydrogen to passivate the bottom of the slab.

| Quantity | Si-EHT | Rel.Err. [%] | Si-Target | $\text{Si-}sp^3d^5s^{*9}$ | Rel.Err. % ⁹ |
|--------------------------------------|--------|--------------|-----------|---------------------------|-------------------------|
| E_c^{Γ} | 3.324 | 1.3 | 3.368 | 3.999 | 0.9 |
| E_v^{Γ} | 0.0 | 0.0 | 0.0 | 0.0 | 0.0 |
| Δ_0 | 0.0445 | 1.0 | 0.045 | 0.0472 | 4.9 |
| $E_{c,min}^{L}$ | 2.393 | 0.3 | 2.400 | 2.383 | 0.7 |
| $E_{c,min}^{X}$ | 1.122 | -0.4 | 1.118 | 1.131 | 1.2 |
| $k_{min}^{[001]}$ | 88.0% | -3.5 | 85.0% | 81.3% | 4.4 |
| $m_{X,l}^{(e)}$ | 0.939 | -2.5 | 0.916 | 0.891 | 2.7 |
| $m_{X,t}^{(e)}$ | 0.161 | 15.5 | 0.190 | 0.201 | 5.8 |
| $m_{L,l}^{(e)}$ | 1.136 | 43.2 | 2.000 | 3.433 | 71.7 |
| $m_{L,t}^{(e)}$ | 0.140 | -39.7 | 0.100 | 0.174 | 74.0 |
| $m_{lh}^{[001]}$ | -0.182 | 10.7 | -0.204 | -0.214 | 4.9 |
| $m_{lh}^{[110]}$ | -0.148 | -0.7 | -0.147 | -0.152 | 3.4 |
| $m_{lh}^{\scriptscriptstyle [1111]}$ | -0.149 | -7.0 | -0.139 | -0.144 | 3.6 |
| $m_{hh}^{[001]}$ | -0.277 | -0.9 | -0.275 | -0.276 | 0.4 |
| $m_{hh}^{[110]}$ | -0.579 | 0.0 | -0.579 | -0.581 | 0.3 |
| $m_{hh}^{[111]}$ | -0.663 | 10.2 | -0.738 | -0.734 | 0.5 |
| m_{so} | -0.217 | 7.1 | -0.234 | -0.246 | 5.1 |
| E_1^G | -12.11 | 3.1 | -12.50 | - | - |
| m_1^G | 1.77 | -47.7 | 1.20 | - | - |

TABLE I: Bandstructure characteristics for bulk silicon using Extended Hückel Theory and spd-orbitals for each Si-atom. The EHT-parameters, cf. Table²⁸ have been optimized to experimental target values²⁹ (4th column). The last two column on the right are the fit values and errors based on an orthogonal tight-binding model using $sp^3d^5s^*$ orbitals.⁹ The effective masses at the *L*-valley are not well established, so that they are to strongly weighted in the optimization.

The lattice vectors for Si(100) (2x1) are $\mathbf{a}_1 = 7.68 \mathring{A} \mathbf{e}_x$ and $\mathbf{a}_2 = 3.84 \mathring{A} \mathbf{e}_y$. Similarly, the Si(111) (2x1) reconstructed surface contains 21 layers with the first 8 layers being relaxed, 12 bulk-like layers, and again the last layer hydrogen passivated. The 2D Bravais lattice vectors here are $\mathbf{a}_1 = 6.65 \mathring{A} \mathbf{e}_x$ and $\mathbf{a}_2 = 3.84 \mathring{A} \mathbf{e}_y$.

Figure 3 shows the bandstructure of reconstructed silicon (100) (2x1) calculated within EHT (top) using the silicon parameters of Table²⁸. The band dispersion at the bottom of Figure 3 correspond to DFT-GW calculations of Rohlfing et al.³² with the π - and π^* -bands in solid lines. As can be seen, our EHT-calculated π - and π^* -surface bands agree very well qualitatively in their shape with DFT-GW calculations as well as with PES experiments for the π -band.

Despite of the good qualitative agreement, which demonstrates the transferability of our parameters in capturing the essential physics of the surface bands, there are quantitative differences. The experimental indirect bandgap $\Delta_{\pi^*-\pi}$ between the π^* and π band, for example, is about $\approx 0.8/0.9$ eV, whereas the gap in EHT is with ≈ 0.3 eV of similar order as in DFT-LDA calculations. In Table II we compare the bandgaps and bandedges calculated in EHT at different points of the 2D Brillouin zone with those obtained by DFT-GW calculations³² and experiments.

The differences between the theoretical approaches become more explicit in Figure 5 where only the E-k dispersion for the π - and π^* -surface bands is shown for the EHT- and the DFT-GW calculation of Rohlfing et al.. ³² The plots have been extracted from Figure 3 by digi-

| | EHT (Table ²⁸ | DFT-GW ³² | Exp. |
|----------------------|--------------------------|----------------------|-----------------------------|
| E_{max}^{π} | 0.47 | 0.16 | -0.42^{33} |
| $E_{min}^{\pi^*}$ | 0.81 | 0.81 | - |
| $\Delta_{\pi^*-\pi}$ | 0.34 | 0.65 | - |
| E^{π}_{Γ} | 0.14 | -0.10 | -0.13^{33} , -0.42^{33} |
| $E_{\Gamma}^{\pi^*}$ | 0.91 | 0.94 | - |
| Δ_{Γ} | 0.78 | 1.04 | - |
| E_J^{π} | -0.20 | -0.19 | -0.26^{33} , -0.26^{33} |
| $E_J^{\pi^*}$ | 1.11 | 1.00 | - |
| Δ_J | 0.91 | 1.19 | - |
| E_K^{π} | -0.74 | -0.81 | -0.97^{33} |
| $E_K^{\pi^*}$ | 1.11 | 1.07 | - |
| Δ_K | 1.85 | 1.87 | - |
| $E_{J'}^{\pi}$ | -0.74 | -0.81 | -0.81^{33} , -0.97^{33} |
| $E_{J'}^{\pi^*}$ | 0.81 | 0.81 | - |
| $\Delta_{J'}$ | 1.55 | 1.61 | - |

TABLE II: Comparison of the bandgaps Δ and bandedges calculated in EHT, DFT-GW,³² and experiments for the silicon surface (100) 2x1 at different points of the 2D Brillouin zone. All values are in units of eV.

tizing the respective π - and π^* -bands. The unoccupied π^* -band agrees quantitatively very well with the one obtained from DFT-GW over the entire Brillouin zone region as shown in Figure 3. Similarly, the π -band matches quantitatively DFT-GW as well over a wide range of the Brillouin zone, except within the $\Gamma-J$ and the first 3rd of the J-K path. The latter domain includes the π -maximum, which appears $\approx 0.25/0.3$ eV too high, so that the $\Delta_{\pi^*-\pi}$ bandgap is noticably underestimated.

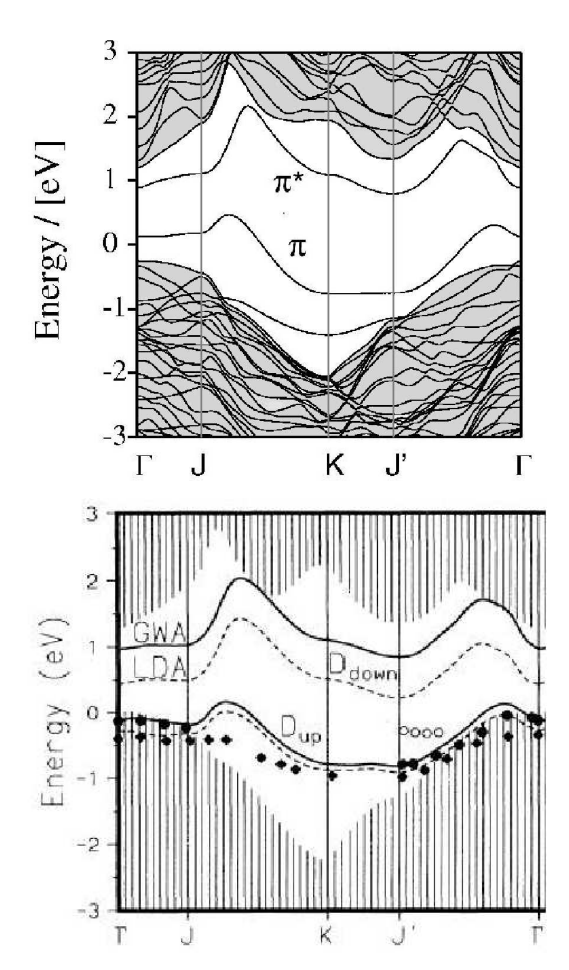


FIG. 3: Surface bandstructure of unpassivated, reconstructed silicon (001) (2x1) calculated within EHT (top) using the parameters of Table²⁸ The figure below is a DFT-GW calculation³². The two bands within the 2D-projected bulk-silicon bandgap correspond to the π and π^* bands of the silicon surface described by the ADM. Reprinted figure (middle) with permission from M. Rohlfing, P. Krüger, and J. Pollmann, PRB, **52**, 1905 (1995). Copyright (1995) by the American Physical Society.

The surface density of states (DOS) is shown in Figure 5. The energy-resolved partial DOS is calculated for each dimer atom (upper and lower) and for the two deeper silicon layers away from the surface. The partial DOS of the upper dimer atom is located more closely to the valence band, whereas for the lower one it is near the conduction band, indicating that the π -surface band is formed from the upper-dimer atom, whereas the π^* -band comes from the lower one 34. Consistent with the π -band dispersion of Figures 3 and 4 the PDOS of the upper dimer atom is too far away from the valence band, so that the π^* - π gap in the PDOS is too small.

Away from the surface and approaching the bulk-like region the weight in the π - and π^* -DOS decreases continuously (layer 4), and completely disappears once a deeper bulk-like layer is reached (layer 8), so that the original bulk-bandgap of ≈ 1.2 eV is recovered.

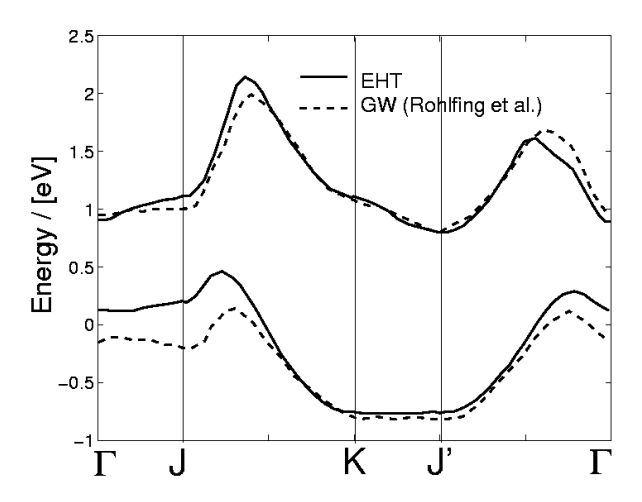


FIG. 4: Comparison of the π - and π^* -surface bands calculated within EHT and DFT-GW³². The dispersion of the π - and π^* -bands of Figure 3 have been digitized. The data of the red curve are adapted with permission from Figure 3 of M. Rohlfing, P. Krüger, and J. Pollmann, PRB, **52**, 1905 (1995). Copyright (1995) by the American Physical Society.

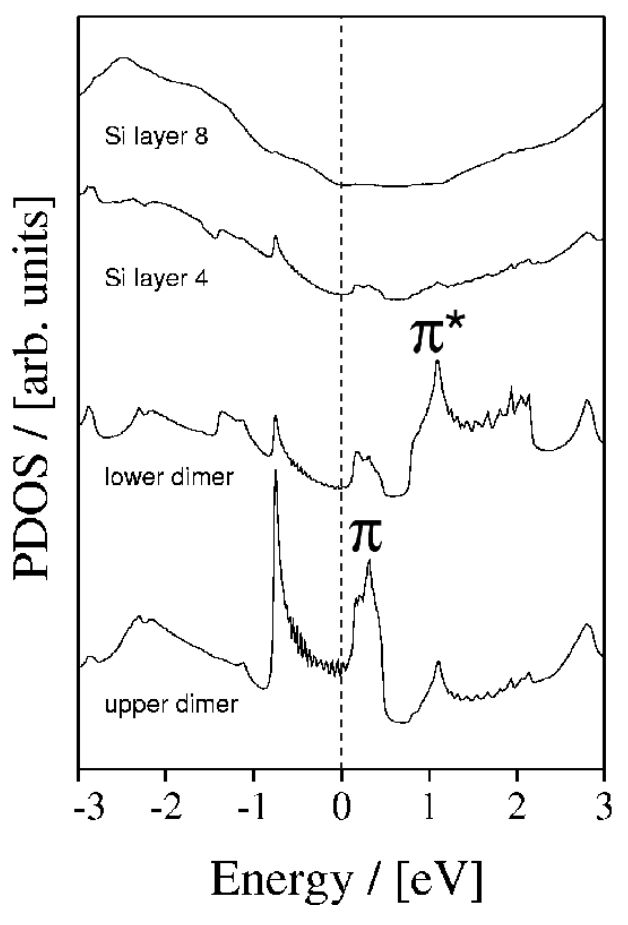
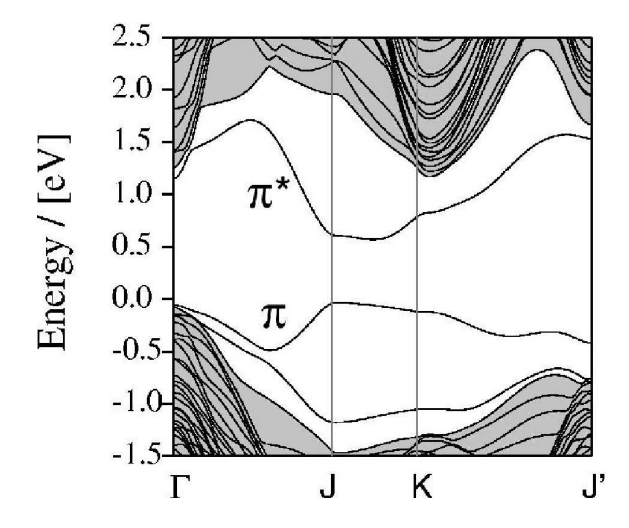


FIG. 5: Density-of-states of un-passivated silicon (100) (2x1) surface calculated for different layers starting from the bulk-like 8th layer (top) towards the (100) surface consisting of the two dimer atoms. The two peaks in the DOS at each dimer atom correspond to the π - and π^* bands.

As second example, we look at the surface bandstructure of reconstructed Si(111) 2x1 as shown in Figure 6 using the EHT-parameters in Table²⁸. Similar to the previous case, the overall shape of the π - and π^* -surface bands match qualitatively well with DFT-GW calculations of Rohlfing et al. 35. In Table III we compare our EHT-bandedges and gaps (1st column) at two specific points J and K of the 2D-Brillouin zone with DFT-GW calculations^{35,36} and PES/IPES experiments. The values for the bandedges as well as for the gaps agree quantitatively well among all three calculations, and show also a good agreement with PES/IPES experiments, where the error in the energy resolution is typically 150 - 200 meVdepending on temperature and incident energy of the electrons. A more extended comparison with PES/IPESexperiments turns out to be very limited, since the π - and the π^* -bands are not as well experimentally determined as in the case of silicon (100) (2x1). Contrary to the pre-



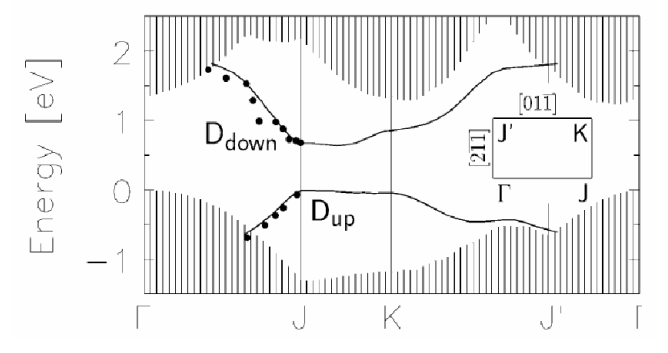


FIG. 6: π - and π^* surface bandstructure of the unpassivated, reconstructed silicon (111) (2x1) calculated in EHT (top). The figure at the bottom shows the dispersion calculated within DFT-GGA of Rohlfing and Louie³⁵, respectively. The bottom figure is reprinted with permission from M. Rohlfing and S.G. Louie, Phys.Stat. Solidi (a), **175**, 17 (1999). Copyright (1999) by the American Physical Society.

vious case of Si(100) (2x1), we find for Si(111) (2x1) that both π^* - and π -band calculated in EHT agree quantitatively very well with DFT-GW calculations of Northrup $et~al.^{36}$ and in particular with Rohlfing $et~al.^{35}$ over the

entire range of the Brillouin zone as shown in Figure 7.

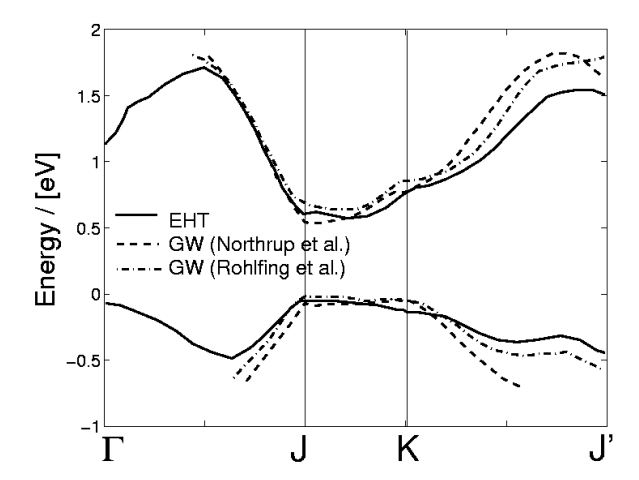


FIG. 7: Comparison of the π - and π^* -surface bands calculated within EHT and DFT-GW^{35,36}. The dispersion of the π - and π^* -bands of Figure 3 have been digitized. The data in the green curve are adapted with permission from Figure 2 of J.E. Northrup, M.S. Hybertsen, and S.G. Louie, Phys.Rev.Lett., **66**, 500 (1991). Copyright (1999) by the American Physical Society. The data in the red curve are adapted with permission from Figure 2 of M. Rohlfing and S.G. Louie, Phys.Stat. Solidi (a), **175**, 17 (1999). Copyright (1999) by the American Physical Society.

| | EHT (Table ²⁸) | DFT-GW ³⁶ | $DFT-GW^{35}$ | Exp. |
|---------------|----------------------------|----------------------|---------------|------|
| Δ_J | 0.66 | 0.60 | 0.68 | - |
| Δ_K | 0.91 | 0.82 | 0.92 | - |
| E_J^{π} | -0.05 | -0.07 | 0.0 | 0.09 |
| $E_J^{\pi^*}$ | 0.61 | 0.53 | 0.69 | 0.67 |
| E_K^{π} | -0.11 | -0.04 | -0.04 | - |
| $E_K^{\pi^*}$ | 0.80 | 0.78 | 0.88 | - |

TABLE III: Comparison of the bandgaps Δ and bandedges (in units of eV) calculated in EHT, DFT-GW^{35,36}, and experiments for the silicon surface (111) (2x1) at different points of the 2D Brillouin zone.

In the two previous cases we explored the transferability of the EHT-parameters, cf. Table²⁸, optimized for bulk-silicon by applying them to other environments such as re-constructed surfaces for silicon (100) (2x1) and (111) (2x1). Without any re-parametrization the experimentally observed π - and π *-surface bands are reproduced qualitatively in their overall shape, and in the case of silicon (111) (2x1) we also achieve a good quantitative match compared to PES/IPES experiments and DFT-GW calculations as well. As discussed, quantitative differences exist, particularly for the indirect bandgap $\Delta_{\pi^*-\pi}$ for silicon (100) (2x1), which is underestimated similar to DFT-LDA pseudopotential calculations.³⁴

One reason for the obvious quantitative differences, particularly the wrong position of the π -band above the valence might be due to the non-self consistent calculation of the bandstructures for the reconstructed silicon

(100) and (111) surfaces. Calculating the total non-self consistent charge on each dimer atom by integrating the LDOS gives a charge of 4.13e on the upper and 3.75e on the lower dimer atom. The total charge of the two dimer atoms is about 7.88e. In turn, a self-consistent calculation of the dimer atom charge using SIESTA, 37,38 results in a total charge on the upper dimer atom of about 4.0e, whereas the lower one has 3.88e. Note, that in the EHT non-scf as well as in the SIESTA scf-case the total charge on the two-dimer system is the same and is effectively positive with respect to their total number of valence electrons of 8. Qualitatively, what one would expect is that the upper dimer atom which carries initially too much negative charge, looses parts of it under self-consistency and charge is transfered partly to the lower dimer atom making, which becomes in turn more negative after self-consistency. The overall effect of self-cinsistency is then mainly to redistribute charge among the two dimer atoms; the initial π -band which consist of the upper (less negative) dimer would float down, whereas the π^* -band would float up since the lower dimer atom is more negative. Both bands float in opposite directions, so that the indirect bandgap $\Delta_{\pi^*-\pi}$ increases.

C. Si-Nanowire $\langle 100 \rangle$: H-Passivation in EHT

As final example, we use the silicon parameters, cf. Table²⁸ in combination with the ones for hydrogen to demonstrate how to passivate surfaces of nanostructures in EHT by means of a silicon nanowire. We use a wire along the $\langle 100 \rangle$ direction with rectangular cross section and sidelength D=1.5 nm as shown in Figure 8. For simplicity we assume that the wire is un-relaxed, i.e. the positions of the silicon atoms of the wire correspond to the positions of bulk silicon. For the surface we consider two cases as illustrated in Figure 8: i) a wire without H-passivation and ii) a wire where we have explicitly added hydrogen atoms to saturate the dangling bonds.

In Figure 9 the 1D-dispersion relation is shown for the two structures, cf. Fig. 8. As can be seen in the left part, the "bulk"-like bandgap of the silicon nanowire is covered by dangling bond states due to the unsaturated bonds of the surface atoms. The entire bands of the dangling bonds are completely removed after the wire is passivated by explicitly attaching hydrogen (bottom), so that the bulk-bandgap of $\approx 2.1~{\rm eV}$ is recovered. Note, that for the case of a H-passivated wire we also assume that the atoms remain in their bulk-positions.

The approach in Extended HückeL Theory to passivate the SiNW surface (and possible other surfaces) by physically attaching hydrogen atoms, for example, differs from the methods described in Ref.³⁹ within an orthogonal tight-binding scheme. In the latter case, the dangling bonds are removed by transforming first the Hamiltonian from a $|s\rangle$, $|p_x\rangle$, $|p_y\rangle$, $|p_z\rangle$ representation to a representation using sp^3 -hybrid basis functions. One then has to

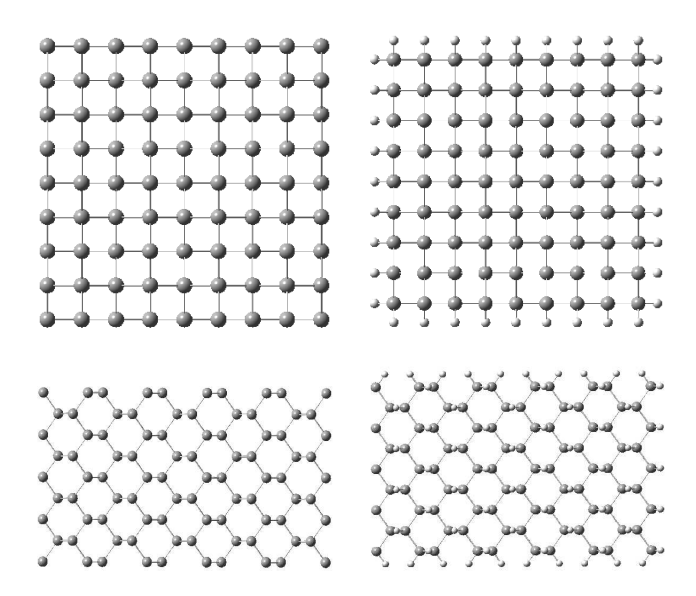


FIG. 8: Front (top) and sideview (bottom) of a silicon nanowire with rectangular cross section and sidelength D=1.5 nm along the $\langle 100 \rangle$ direction. For the un-passivated wire (left) the unit cell contains 81 silicon atoms, and in the H-passivated case (right) the total number of atoms is 117.

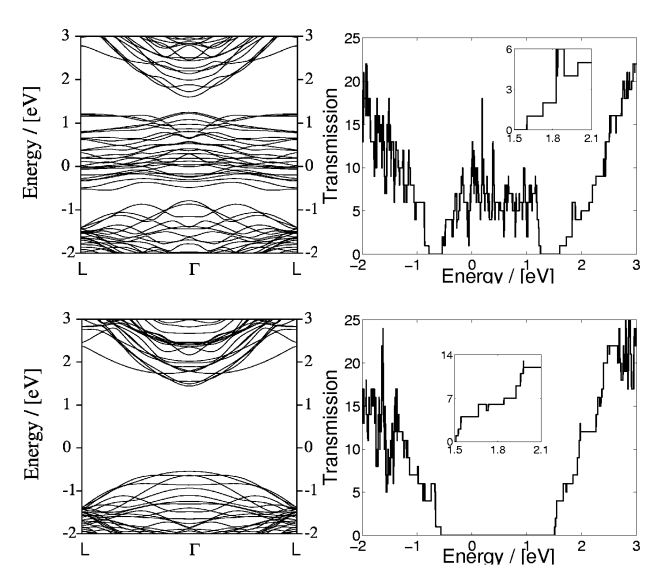


FIG. 9: 1D bandstructure and transmission per spin of an un-relaxed silicon nanowire along the $\langle 100 \rangle$ wire axis. The E-k and transmission on the left are for the unpassivated surface, and on the right the surface is hydrogen passivated to remove the dangling bond states. The transmission shown in the insets takes integer values where each channel contributes one unit quantum conductance $G_0 = e^2/h$ per spin.

check which bonds of the surface atoms are not saturated and to increase then the respective orbital energy of the dangling bond. In raising the orbital energy manually one formally mimics the effect of the hydrogen atoms onto the silicon surface atoms as if hydrogen were attached. The amount, however, by which the dangling bond state energy has to be shifted is *a priori* not known and has to be determined empirically³⁹.

In turn, in Extended Hückel Theory the surface passivation is controlled by the passivation atoms, which are an explicit part of the entire structure. Once the structure is specified, the amount by which the silicon levels are shifted is determined by the chemical species of the passivation atoms. The hybridization causing the shift of the silicon dangling bond states is naturally incorporated within the Hamiltonian matrix through the EHT-prescription, cf. Eq.(1).

IV. SUMMARY

We applied Extended Hückel Theory (EHT) to describe the electronic structure of several silicon-based structures. A quantitative benchmark of the bulk-silicon electronic structure was achieved by optimizing the EHT-parameters to experimentally determined target values specific for the bulk-bandstructure of silicon. Our developed parameter set for silicon provides a quantitative good agreement with these targets and are competitive with the results based on orthogonal-tight binding for silicon.

The transferability of the parameter set was investigated by applying them to different environments such as reconstructed silicon for two different surface orientations. Within our EHT-approach using the bulkoptmized parameters we could reproduce the essential features of the surface band dispersion, in particular the π - and π *-surface bands experimentally well established. A quantitative comparison of our EHT-bandstructure with DFT-GW calculations as well as PES/IPES experiments shows qualitative and quantitative agreement, particularly for silicon (111) (2x1) surface. However, our indirect bandgap $\Delta_{\pi^*-\pi}$ is lower compared to PES/IPES experiments and of the same order as DFT-LDA calculated gaps. This discrepancy is partly due to the non-self consistent calculation of the surface electronic structure of reconstructed silicon, where the charge redistribution due to structural changes is discarded. We expect that a full 3D self-consistent solution of the electronic structure, for example within a Complete Neglect of Differential Overlap scheme (CNDO), can correct for the discrepancies, which would further increase the transferability of our EHT-parameters for silicon.

Using the silicon nanowire as example we used the EHT-parameters for silicon and demonstrated a generic approach to surface passivation of nanostructure materials by physically attaching hydrogen atoms to the SiNW surface. The respective dangling bond states are removed

from the bandgap region of the wire in a systematic manner without the need to shift dangling bond molecular levels by hand.

The flexibility of EHT demonstrated here and in our previous paper (Part I)¹⁸ opens the door to study electronic structure and transport through molecular heterostructures as well as larger nanostructures preserving the atomistic features of the system. We believe, that Extended Hückel Theory is a good practical comprimise between rigorous, but computationally expensive DFTbased approaches, and orthogonal tight-binding methods, which might not be suitable for large structural deformations beyond 2-3%. More coarse-grained models such as effective mass might be even prohibitive for the same purpose, since they inherently fail to account for bonding. The main appeal of EHT is that it does capture bulk- as well as surface physics along with bonding chemistry at heterointerfaces and molecular heterostructures including large structural deformations - all within a unified semi-empirical framework 18,22,40. Silicon nanowires, for example, are interesting candidates for new channel materials for novel MOSFETs. A widely discussed and still open question is whether structural relaxation of the wire significantly affects its electronic structure as well as the overall device performance. Intuitively, one expects that the electronic properties particularly of small diameter wires are dictated by their surface. Some aspects of this problem is currently investigated where we employ Extended Hückel Theory to describe the electronic structure of the relaxed wire for different diameters and orientations. 41 Extended Hückel Theory as it stands also needs further improvement to fully utilize its capabilities and to establish it as a methodological tool towards a quantitative modeling of quantum transport through nanostructures. This is left for future work.

Acknowledgement

We acknowledge the support of the Army Research Office through the Defense University Research Initiative in Nanotechnology (DURINT) program, the Defense Advanced Research Projects Agency-Air Force Office of Scientific Research (DARPA-AFOSR). J. Cerda acknowledges support from the Spanish DGICyT under contract No. MAT2004-05348-C04-2, respectively. We further acknowledge the Network for Computational Nanotechnology (NCN) to use the computational facilities. We are indebted to Prof. Tim Boykin for helpful discussions. The authors would also like to thank S. Srivastava for helpful discussions.

N. P. Guisinger et al., "Room Temperature Negative Differential Resistance through Individual Organic Molecules

on Silicon Surfaces" Nano.Lett., 4, 55 (2004).

² R.G. Parr and W. Yang, Density-Functional Theory of

Atoms and Molecules New York: Cambridge University Press, 1994.

³ U. von Barth, "Basic Density Functional Theory - an Overview," Physica Scripta, **T109**, 9 (2004).

⁴ R.M. Martin, Electronic Structure: Basic Theory and Practical Methods New York: Cambridge University Press, 1994.

W. Lu, V. Meunier, and J. Bernholc, "Nonequilibrium Quantum Transport Properties of Organic Molecules on Silicon" Phys.Rev.Lett., 95, 206805 (2005).

⁶ M. Rohlfing, P. Krüger, and J. Pollmann, "Quasiparticle band-structure calculations for C, Si, Ge, GaAs, and SiC using Gaussian-orbital basis sets" Phys.Rev.B, 48, 17791 (1993).

⁷ P. Vogl, H.P. Hjalmarson, and J.D. Dow, "A Semi-Empirical Tight-Binding Theory of the Electronic Structure of Semiconductors" <u>J.Phys.Chem.</u> Solids, 365 44, (1983).

⁸ J.-M. Jancu, R. Scholz, F. Beltram, and F. Bassani, "Empirical spds* tight-binding calculation for cubic semiconductors: General method and material parameters" Phys.Rev.B, 57, 6493 (1998).

 9 T.B. Boykin, G. Klimeck, and F. Oyafuso, "Valence band effective mass expressions in the $sp^3d^5s^*$ empirical tight-binding model applied to a Si and Ge parametrization" Phys.Rev.B, **69**, 115201 (2004).

¹⁰ D. J. Chadi, "Energy-Minimization Approach to the Atomic Geometry of Semiconductor Surfaces" Phys.Rev.Lett, 41, 1062 (1978).

¹¹ D. J. Chadi, "Atomic and Electronic Structures of Reconstructed Si(100) Surfaces" Phys.Rev.Lett., 43, 43 (1979).

D. J. Chadi, "Atomic Structure of Si(111) Surfaces" Surf.Sci., 99, 1 (1980).

¹³ G. V. Hansson et al., "Electronic Structure of Si(111) Surfaces" Surf.Sci., 99, 13 (1980).

¹⁴ D. J. Chadi, "Semiconductor Surface Reconstruction" Vacuum, 33, 613 (1983).

D. J. Chadi, "Energy-Minimization Approach to the Atomic Geometry of Semiconductor Surfaces" Surf.Sci., 299, 311 (1994).

¹⁶ Z.M. Khakimov, P.L. Tereshchuk, N.T. Sulaymanov, F.T. Umarova, and M.T. Swihart, "Nonconventional tight-binding method for the calculation of the total energy and spectroscopic energies of atomic clusters: Transferable parameters for silicon" Phys.Rev.B, 72, 115335 (2005).

¹⁷ S.T. Pantelides and J. Pollmann, "Critique of the Empirical Tight-Binding Method for Surfaces and Interfaces" J.Vac.Sci.Technol., **16**, 1349 (1979).

¹⁸ D. Kienle, J.I. Cerda, and A.W. Ghosh, "Extended Hückel theory for bandstructure, chemistry and transport. I. Carbon Nanotubes" (submitted).

¹⁹ J.C. Slater and G.F. Koster, "Simplified LCAO Method for the Periodic Potential Problem," <u>Phys.Rev.</u>, **94**, 1498 (1954).

²⁰ J.N. Murrell and A.J. Harget, <u>Semi-empirical self-consistent-field molecular orbital theory of molecules New York: Wiley-Interscience</u>, 1972.

J. Cerda and F. Soria, "Accurate and transferable extended Hückel-type tight-binding parameters," Phys.Rev.

B, **61**(12), 7965 (2000).

D. Kienle and A.W. Ghosh, "Atomistic Modeling of Metal-Nanotube Contacts" J.Comp.El., 4, 97 (2005).

²³ H. Raza, K. Bevan, T. Kazmi, D. Kienle, A.W. Ghosh, and S. Datta, "The Role of localized States in Transport at molecular Scale" (in preparation).

²⁴ C. M. Goringe, D.R. Bowler, and E. Hernandez, "Tight-Binding Modelling of Materials" <u>Rep. Prog. Phys.</u>, **60**, 1447 (1997)

A. Peccia and Aldo Di Carlo, "Atomistic Theory of Transport in Organic and Inorganic Nanostructures" Rep.Prog.Phys., 67, 1497 (2004).

²⁶ P.N. Keating, "Effect of Invariance Requirements on the Elastic Strain Energy of Crystals with Application to the Diamond Structure," Phys.Rev., 145, 637 (1966).

 27 www.icmm.csic.es/jcerda/index.html.

The EHT-parameters for silicon are provided upon request from the author via email: kienle@ecn.purdue.edu

The EHT-parameters forbulk silicon have been optimized to experimental target values taken from Semiconductors: Group IV Elements and III-V Compounds, Editor: O. Madelung, New York: Springer, 1991.

³⁰ A. Ramstad, G. Brocks, and P.J. Kelly, "Theoretical study of the Si(100) surface reconstruction" <u>Phys.Rev.B</u>, **51**, 14504 (1995).

³¹ G. Xu, B. Deng, Z. Yu, S.Y. Tong, A.A. Van Hove, F. Jona, and I. Zasada, "Atomic structure of the cleaved Si(111)-(2x1) surface refined by dynamical LEED" <u>Phys.Rev.B</u>, 70, 045307 (2004).

M. Rohlfing, P. Krüger, and J. Pollmann, "Efficient scheme for GW quasiparticle band-structure calculations with applications to bulk Si and to the Si(001)-(2x1) surface" Phys.Rev.B, 52, 1905 (1995).

³³ The experimental values have been extracted from the respective figures.

³⁴ G.P. Srivastava, <u>Theoretical Modelling of Semiconductor Surfaces</u>, Singapore: World Scientific, 1999.

M. Rohlfing and S.G. Louie, "Optical reflectivity of the Si(111)-(2x1) surface - the role of the electron-hole interaction" Phys.Stat. Solidi (a), 175, 17 (1999).

³⁶ J.E. Northrup, M.S. Hybertsen, and S.G. Louie, "Many-Body Calculation of the Surface-State Energies for Si(111) 2x1" Phys.Rev.Lett., 66, 500 (1991).

³⁷ Self-consistent order-N density-functional calculations for very large systems, P. Ordejon, E. Artacho, and J. M. Soler, Phys.Rev.B (Rapid Comm.) **53**, R10441 (1996).

J.M. Soler, E. Artacho, J.D. Gale, A. Garcia, J. Junquera, P. Ordejon, and D. Sanchez-Portal "The Siesta method for ab initio order-N materials simulation," <u>J</u>. Phys.: Cond. Mat., 14, 2745 (2002).

³⁹ S. Lee, F. Oyafuso, P. von Allmen, and G. Klimeck, "Boundary conditions for the electronic structure of finiteextent embedded semiconductor nanostructures" <u>PRB</u>, **69**, 045316 (2004).

 40 G.C. Liang and A.W. Ghosh, "Identifying Contact Effects in Electronic Conduction through C_{60} on Silicon," Phys.Rev.Lett., **95**, 076403 (2005).

 41 $\overline{\mathrm{G.C.}}$ Liang $\underline{\mathrm{e}}\mathrm{t}$ al. (in preparation)